Zinc-Modified UiO-66 for Reversible SO_2 Capture with High Structural Stability

Nishesh Kumar Gupta[a,b*], Kwang Soo Kim[b]

[a]Faculty of Civil and Environmental Engineering, Technion−Israel Institute of Technology, Haifa 32000, Israel.

[b]Department of Environmental Research, University of Science and Technology (UST), Daejeon 34113, Korea.

*Email: nishesh0602@gmail.com

Received: 24.9.2025, Revised: 11.10.2025 Accepted: 14.10.2025

Abstract

A zinc-modified zirconium-based MOF, UiO-66-Zn, was synthesized via a one-step solvothermal method and evaluated for SO_2 capture. Structural characterizations (PXRD, FT-IR, XPS, and TEM) confirmed successful Zn incorporation without compromising the UiO-66 framework integrity. UiO-66-Zn exhibited a BET surface area of 597 m^2 g^{-1} and achieved a maximum SO_2 uptake of 4.94 mmol g^{-1} at 298 K and 1 bar. Notably, significant adsorption occurred at low pressures (0-0.01 bar), indicating possible Zn–SO_2 interactions. Post-adsorption analyses revealed preserved crystallinity and reversible adsorption, with no permanent sulfur species detected. These findings highlight UiO-66-Zn as a robust and efficient sorbent with high capacity, stability, and regenerability, making it a promising material for practical desulfurization application

Keywords: Metal-organic frameworks (MOFs); UiO-66-Zn; SO_2 adsorption; Structural stability; Desulfurization

1.Introduction

UiO-66 (Universitetet i Oslo), a zirconium-based metal–organic framework (MOF), consists of $[Zr_6O_4(OH)_4]$ clusters connected by 1,4-benzodicarboxylate linkers. It is among the most

DOI: 10.59143/isas.jisas.4.2.EIOO9718

extensively studied MOFs due to its high stability, straightforward synthesis, and permanent porosity. These features have enabled applications in gas storage, separation, and catalysis [1–3].

The Zr–O(linker) coordination in UiO-66 provides suitable metal–donor interactions for the adsorption of acidic gases such as sulfur dioxide (SO_2). Moreover, UiO-66 exhibits exceptional structural stability even in the presence of acidic gases and competing water molecules [4]. SO_2 is a toxic gas associated with respiratory illnesses and is a major precursor of $PM_{2.5}$. While natural events contribute to SO_2 emissions, anthropogenic sources, particularly fossil fuel combustion and industrial processes, are the primary contributors. Removal of SO_2 at low concentrations (500–3000 ppm) from flue and natural gas streams remains a significant challenge.

Previous studies have shown that functional modification of UiO-66 enhances its SO_2 adsorption capacity. De Coste [5] et al. reported that UiO-66 analogues with free –COOH groups exhibited uptake of 0.8 mmol g^{-1} at 375 ppm SO_2, compared with 0.1 mmol g^{-1} for unmodified UiO-66. Walton [6] et al. demonstrated that cyanoacetic acid-modulated UiO-66 achieved a similar uptake at 950 ppm SO_2, attributed to chalcogen bonding interactions. Qu et al[7]. reported an enhanced SO_2 uptake capacity for UiO-66 upon functionalization with varying numbers of amine groups within the framework skeleton. The introduction of amine functionalities increased the interaction strength between SO_2 molecules and the framework, thereby improving adsorption performance. Yang [8] et al. investigated metal–catechol group-modified UiO-66 (UiO-66-Cat(M)) for SO_2 capture and, through theoretical analysis, demonstrated that modification with different metal–catechol complexes enhanced SO_2 affinity. Although the various metal–catechol modifications exhibited comparable SO_2 uptake capacities, UiO-66-Cat(Zn) showed the lowest adsorption energy, suggesting that Zn-functionalization is particularly favorable for reversible SO_2 adsorption. These studies highlight that introducing suitable functional sites can strengthen host–guest interactions and improve SO_2 capture performance.

In this context, a metal ion (Zn^{2+}) incorporation into the UiO-66 framework has been explored to enhance its affinity toward SO_2. Zinc centers can act as Lewis acidic sites capable of forming strong coordination or electrostatic interactions with the oxygen atoms of SO_2, leading to greater affinity and improved adsorption [9–11]. Here, we have synthesized UiO-66-Zn via a one-step solvothermal reaction using Zr-Zn salts and terephthalic acid. The MOF was characterized using microscopic and spectroscopic methods to examine its morphology and physicochemical properties. SO_2 adsorption was tested at 298 K, and the structural stability of the framework was

confirmed post SO_2 exposure. UiO-66-Zn exhibited high SO_2 uptake at 1 bar and 298 K while maintaining structural integrity, indicating its potential for desulfurization applications.

2. Materials and methods

2.1 Chemicals

Zinc chloride, zirconium tetrachloride, terephthalic acid, N,N-dimethylformamide (DMF), N,N-diethylformamide (DEF), and acetone were obtained from Sigma-Aldrich. All reagents were of analytical grade and used as received without further purification.

2.2 Synthesis of UiO-66-Zn

UiO-66-Zn was synthesized via a solvothermal method. $ZnCl_2$ (0.21 g), $ZrCl_4$ (0.36 g), and H_2BDC (0.25 g) were dissolved in 10 mL of DEF to obtain a clear solution, which was transferred to a Teflon-lined autoclave and heated at 393 K for 72 h. The resulting white solid was collected and washed with DMF (5 mL, 4 times), followed by solvent exchange with acetone (two times over two days). The MOF was dried at 343 K before gas adsorption measurement.

2.3 Analytical instruments

The surface morphology of the MOF was examined by scanning electron microscopy (SEM, Hitachi S-4800, Japan). A dried, finely ground sample was coated with a gold-platinum alloy using an ion sputter coater (Hitachi E-1048). Elemental distribution was analyzed by energy-dispersive X-ray spectroscopy (EDS, X-Maxn 80 T, Oxford, UK). Transmission electron microscopy (TEM) images were obtained using a field-emission TEM (JEM-2100F, JEOL, Japan). N_2 adsorption-desorption isotherm was collected at 77 K using a Micromeritics Gemini 2360 analyzer after degassing the sample at 473 K for 2 h (Micromeritics FlowPrep 060). Powder X-ray diffraction (PXRD) patterns were collected on a Rigaku D/Max-2500 diffractometer with Cu Kα radiation and a Ni filter at a scan rate of 3° min^{-1}. Fourier-transform infrared (FTIR) spectra were recorded on a PerkinElmer spectrometer using KBr pellets, with 60 scans collected at a resolution of 0.02 cm^{-1}. X-ray photoelectron spectroscopy (XPS) was performed on a Thermo Scientific K-Alpha instrument (UK) equipped with a monochromatic Al Kα source under a base pressure of 4.8×10^{-9} mbar.

2.4 SO_2 adsorption studies

The SO_2 adsorption isotherm was measured gravimetrically using a Dynamic Vapor Sorption (DVS Vacuum, Surface Measurement Systems Ltd.) analyzer. Before measurement, MOF was activated at 423 K under dynamic vacuum (1×10^{-8} bar) for 6 h. Adsorption experiments were performed at 298 K up to 1 bar.

3 Results and discussion

3.1 Characterization of UiO-66-Zn

The surface morphology of UiO-66-Zn was examined using SEM (**Fig. 1a**). The SEM image reveals aggregated polyhedral particles with irregular sheet-like and cube-like morphologies, consistent with the nanoscale crystalline features of MOFs. Elemental mapping from SEM-EDS further confirms the homogeneous distribution of C, O, Zr, and Zn throughout the framework, indicating successful incorporation of Zn into the UiO-66 structure without noticeable phase segregation. TEM provided further insights into the structural features of UiO-66-Zn (**Fig. 1b**). The TEM image clearly shows nano-sized cubes (particle size < 100 nm) and thin sheet-like particles, which are in agreement with the morphological features observed in SEM. Such a dual morphology is well-documented in the literature for MOFs [12]. The EDX spectrum demonstrates the presence of the expected elements (C ~80.4%, O ~18.2%, Zr ~1.2%, and Zn ~0.2%), further confirming the composition of the synthesized MOF. Elemental mapping also shows a uniform distribution of all constituent elements, corroborating the successful inclusion of Zn within the UiO-66 matrix.

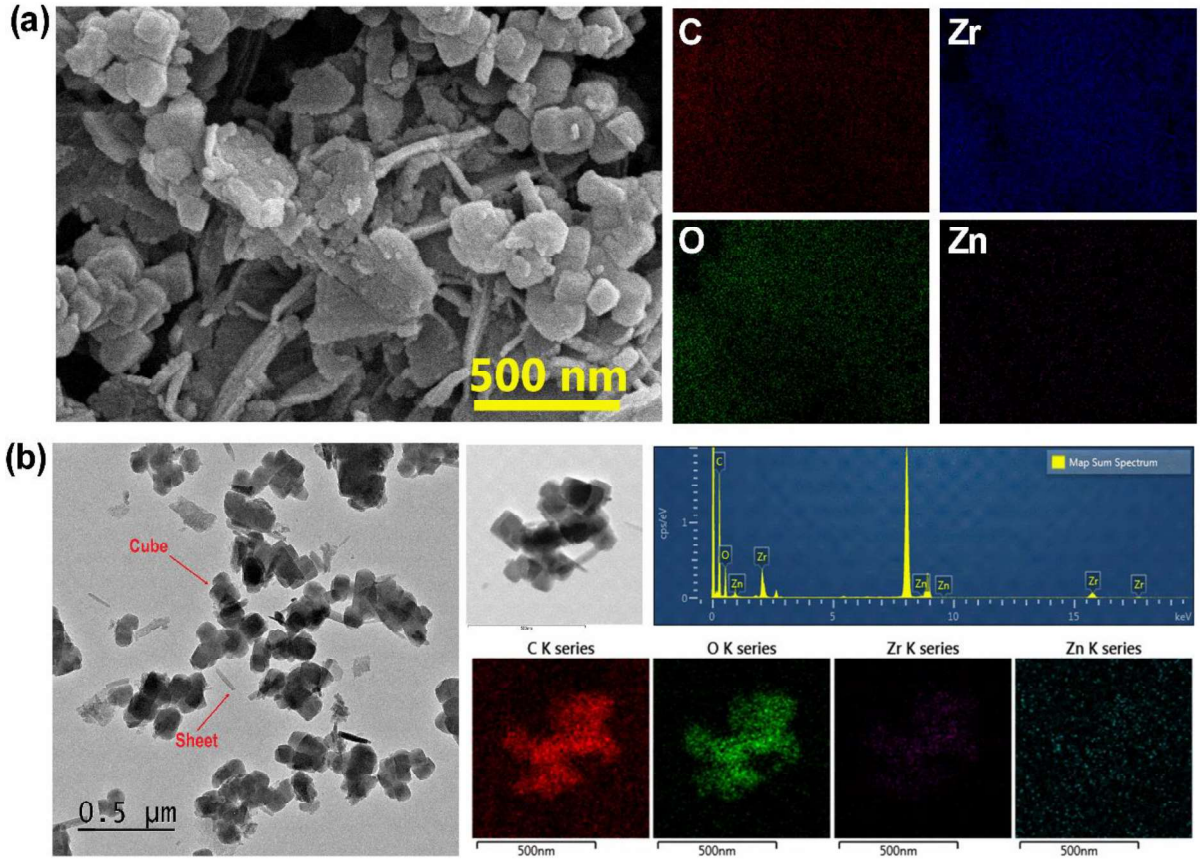

Fig. 1 (**a**) SEM micrograph and SEM-EDS mapping; (**b**) TEM micrograph and EDX mapping of UiO-66-Zn.

The crystallinity and phase purity of the synthesized UiO-66-Zn were confirmed by PXRD analysis (**Fig. 2a**). The diffraction peaks of UiO-66-Zn closely match those of simulated UiO-66 (CCDC 837796), with slight broadening attributed to nanoscale crystallite size, while no impurity peaks corresponding to MOF-5 (CCDC 256965) were observed. This confirms the successful incorporation of Zn into the UiO-66 framework without altering its characteristic topology. The porosity of UiO-66-Zn was evaluated by N_2 adsorption-desorption analysis at 77 K (**Fig. 2b**). The isotherm exhibits a type IVa isotherm, which is a commonly observed feature for materials containing mesopores [13]. The Brunauer–Emmett–Teller (BET) surface area was calculated to be 597 $m^2\ g^{-1}$, with a total pore volume of 0.44 $cm^3\ g^{-1}$.

The functional groups present in UiO-66-Zn were analyzed by FT-IR spectroscopy (**Fig. 2c**). Multiple bands in the 1200-1000 and 1000-700 cm^{-1} region correspond to the in-plane and out-of-plane C–H bending modes, respectively. The band at 1500 cm^{-1} was for the aromatic C=C

skeleton. The band for the acidic C=O stretching vibrations was observed at 1656 cm^{-1} along with the bands at 1584 and 1395 cm^{-1} for asymmetric and symmetric stretching of O–C–O, respectively. The band around 553 cm^{-1} was attributed to the Zr–O(C) linkage [14]. X-ray photoelectron spectroscopy (XPS) survey spectrum further validated the elemental composition of UiO-66-Zn (**Fig. 2d**). The prominent peaks at binding energies corresponding to O 1s, C 1s, and Zr 3p confirm the UiO-66 framework. Since Zn constitutes only 0.22 atomic% of the total composition, its signal is not clearly visible in the survey spectrum; therefore, high-resolution XPS analysis was carried out to confirm the presence of Zn.

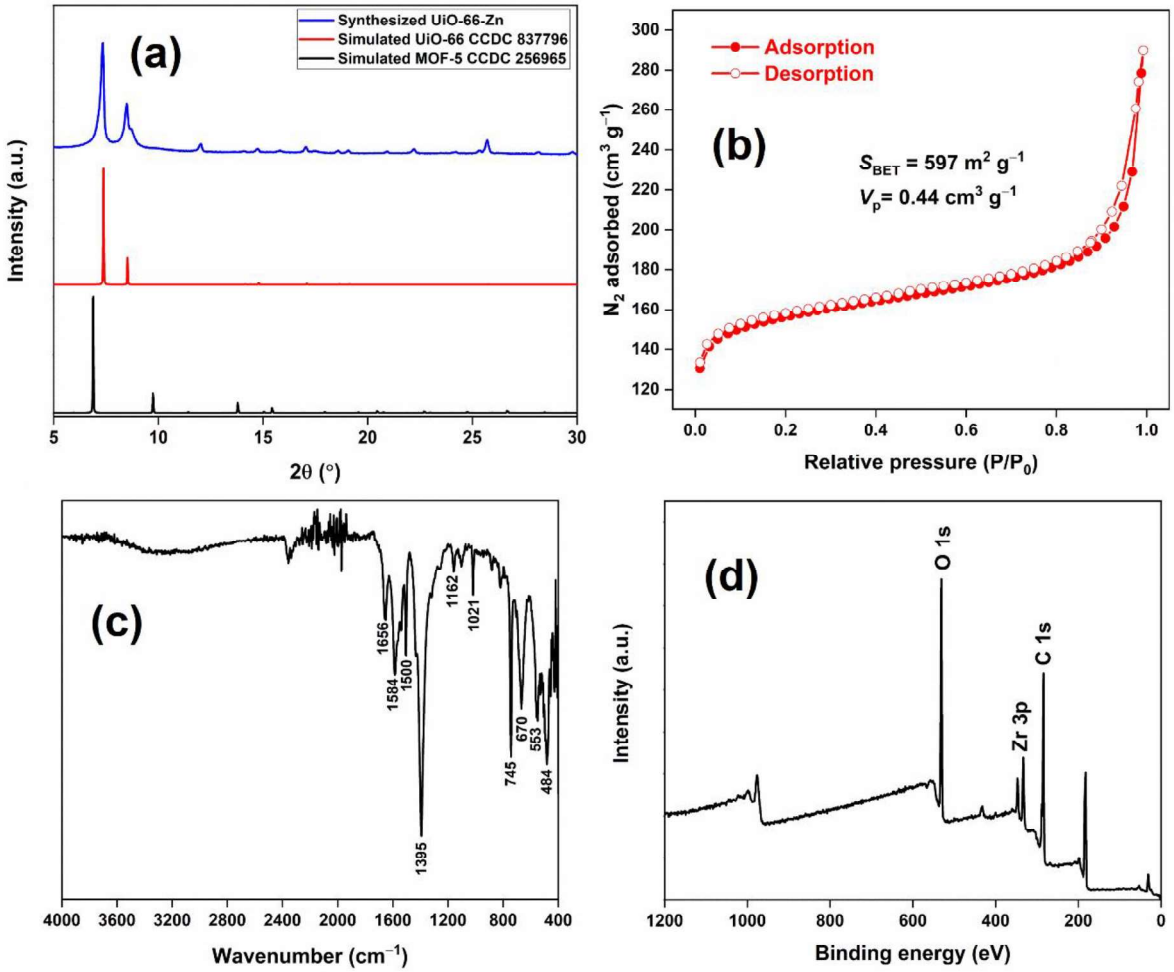

Fig. 2 (**a**) PXRD pattern; (**b**) N_2 adsorption-desorption isotherm at 77 K; (**c**) FT-IR spectrum; (**d**) XPS survey scan of UiO-66-Zn.

High-resolution XPS spectra were collected to gain detailed insight into the chemical states of UiO-66-Zn. The deconvoluted C 1s spectrum (**Fig. 3a**) shows peaks at 284.2 eV and 288.1 eV, corresponding to C–C/C=C bonds and carboxylate (O–C=O) groups, respectively, which are characteristic of the terephthalate linker. The O 1s spectrum (**Fig. 3b**) displays a major peak at 531.2 eV, attributed to metal–oxygen bonds within the Zr–O/Zn–O clusters. The Zr 3d region (**Fig. 3c**) exhibits two distinct peaks at 182.2 eV and 184.5 eV, assigned to Zr $3d_{5/2}$ and Zr $3d_{3/2}$, confirming the +4 oxidation state of zirconium in the framework [15]. Importantly, the Zn 2p spectrum (**Fig. 3d**) reveals peaks at 1021.6 eV (Zn $2p_{3/2}$) and 1044.7 eV (Zn $2p_{1/2}$), which are consistent with Zn^{2+} species, validating the successful incorporation of Zn^{2+} into the UiO-66 structure [16]. These findings, combined with the survey spectrum, provide clear evidence of Zn coordination within the MOF while maintaining the UiO-66 backbone.

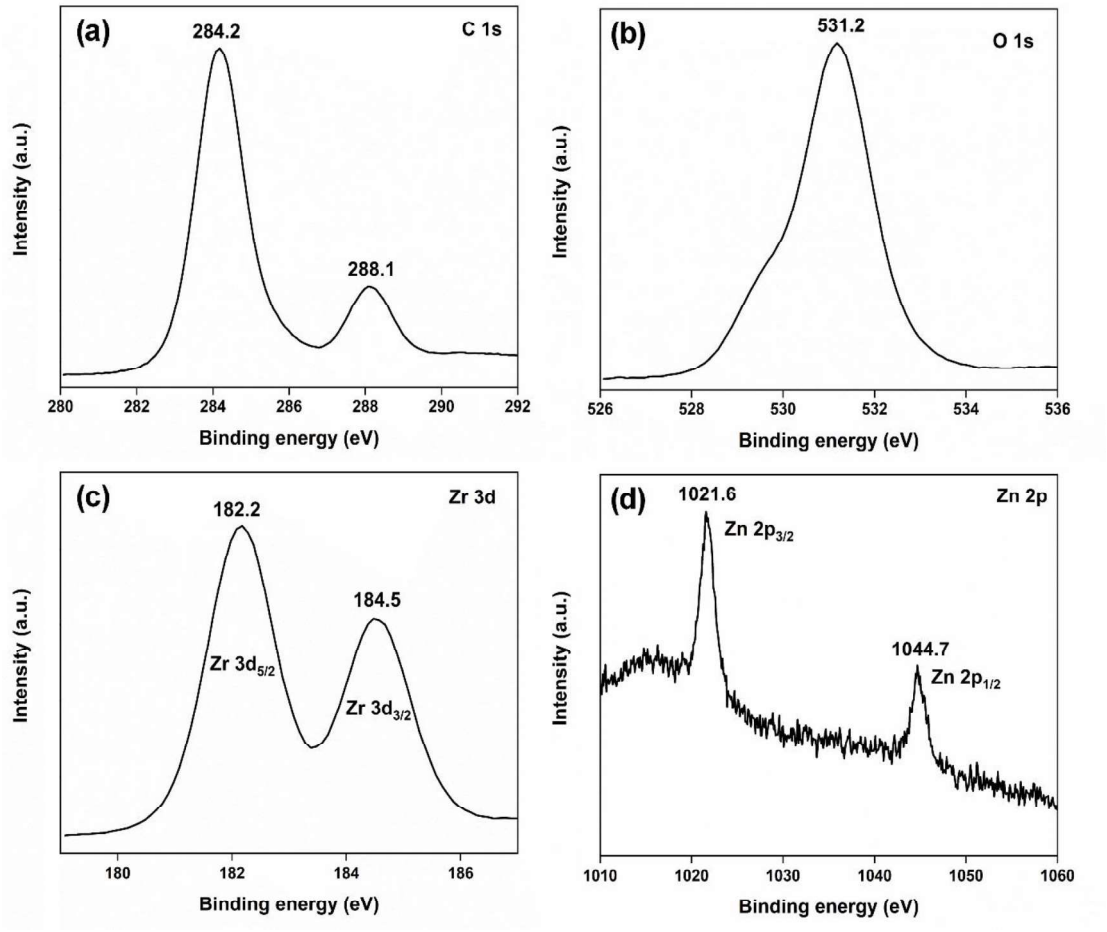

Fig.3 High-resolution (a) C 1s; (b) O 1s; (c) Zr 3d; (d) Zn 2p spectra of UiO-66-Zn.

3.2 SO_2 breakthrough study

SO_2 adsorption-desorption isotherms were recorded at 298 K after activation. The SO_2 isotherms reflected a steady rise in the uptake with increasing pressure without reaching the saturation stage at 1.0 bar (**Fig. 4**). The maximum SO_2 adsorption capacity at 1 bar and 298 K was 4.94 mmol g^{-1}, which was comparable to other reported Zr-MOFs like Zr-Fumarate (600 m^2 g^{-1}, 4.9 mmol g^{-1}) [17] and MFM-600(Zr) (2281 m^2 g^{-1}, 5.0 mmol g^{-1}) [18]. Since the low-pressure range has practical relevance for the desulfurization of flue gases, we have decided to study the SO_2 uptake behavior in the 0-0.01 bar region (**Fig. 4 inset**). The maximum adsorption capacity at 0.01 bar was 0.68 mmol g^{-1}. The strong interaction of SO_2 with Zn sites at low pressures, along with hydrogen bonding between μ_3-OH groups and the oxygen atoms of SO_2 (μ-$OH^{\delta+}\cdots^{\delta-}OSO$), indicates that the overall SO_2 uptake behavior results from the synergistic effects of physical and chemical adsorption mechanisms[19]. The maximum adsorption capacity of UiO-66-Zn at 0.01 bar and 298 K was similar to highly porous Zr-MOFs like DUT-67(Zr) (1260 m^2 g^{-1}, 0.7 mmol g^{-1}) and NU-1000 (1740 m^2 g^{-1}, 0.6 mmol g^{-1}) in similar experimental conditions [17]. The comparison of SO_2 adsorption capacity at 0.01 bar with other reported MOFs showed similar or superior performance for the synthesized UiO-66-Zn (**Table 1**).

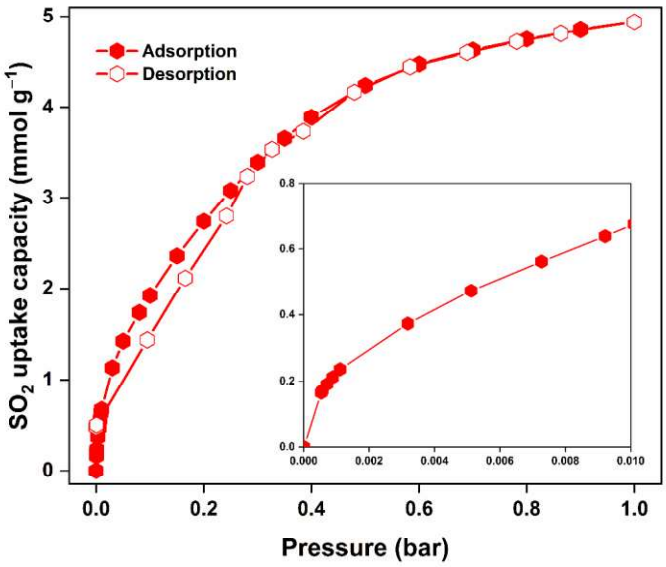

Fig. 4. SO_2 adsorption-desorption isotherms for UiO-66-Zn (**Inset:** adsorption isotherm in the 0-0.01 bar region).

Table 1. Comparison of SO_2 adsorption at 0.01 bar in MOFs.

MOF	Surface area ($m^2\ g^{-1}$)	Temperature (K)	Uptake capacity (mmol g^{-1})	
			0.01 bar	1.0 bar
DUT-67(Zr)	1260	293	0.7	9.0
NU-1000	1740		0.6	12.2
MIL-100(Al)	1890		0.4	16.3
MIL-53(Al)-BDC	1450		0.4	10.5
MIL-53(Al)-TDC [17]	1000		0.6	6.9
Fe(BTC)	1070	293	0.6	9.5
ZIF-8	1820		0.1	8.2
ZIF-67 [20]	1980		0.1	11.0
MOF-177 [11]	4100	293	0.3	25.7
[RuGa]@NU-1000 [21]	1796	298	0.5	7.5
ELM-12 [22]	706	298	0.7	2.7
CPL-1 [23]	335	298	0.5	2.0
MIL-101 [24]	3217	298	0.6	24.4
UiO-66-Zn	**597**	**298**	**0.7**	**4.9**

3.3 MOF stability

The structural stability of UiO-66-Zn before and after SO_2 adsorption was investigated using PXRD (**Fig. 5a**). The diffraction patterns of pristine and SO_2-exposed UiO-66-Zn (UiO-66-Zn_SO_2) show no significant differences, confirming that the crystallinity and framework integrity were well preserved during the SO_2 uptake process. FT-IR spectra (**Fig. 5b**) further support this observation, with both samples exhibiting the characteristic vibrations of the terephthalate linker, indicating high structural stability of the MOF. These results suggest that UiO-66-Zn remains structurally intact and is a promising candidate for desulfurization applications. Further insights into the chemical environment after SO_2 exposure were obtained from XPS analysis. The Zn $2p_{3/2}$ and Zn $2p_{1/2}$ peaks exhibited only minor shifts, indicating an insignificant change in the Zn coordination environment, while the S 2p spectrum showed no

significant sulfur-related signals (**Fig. 5 c, d**). This confirms that the additional SO_2 binding sites in UiO-66-Zn remain intact and that the adsorption process is fully reversible.

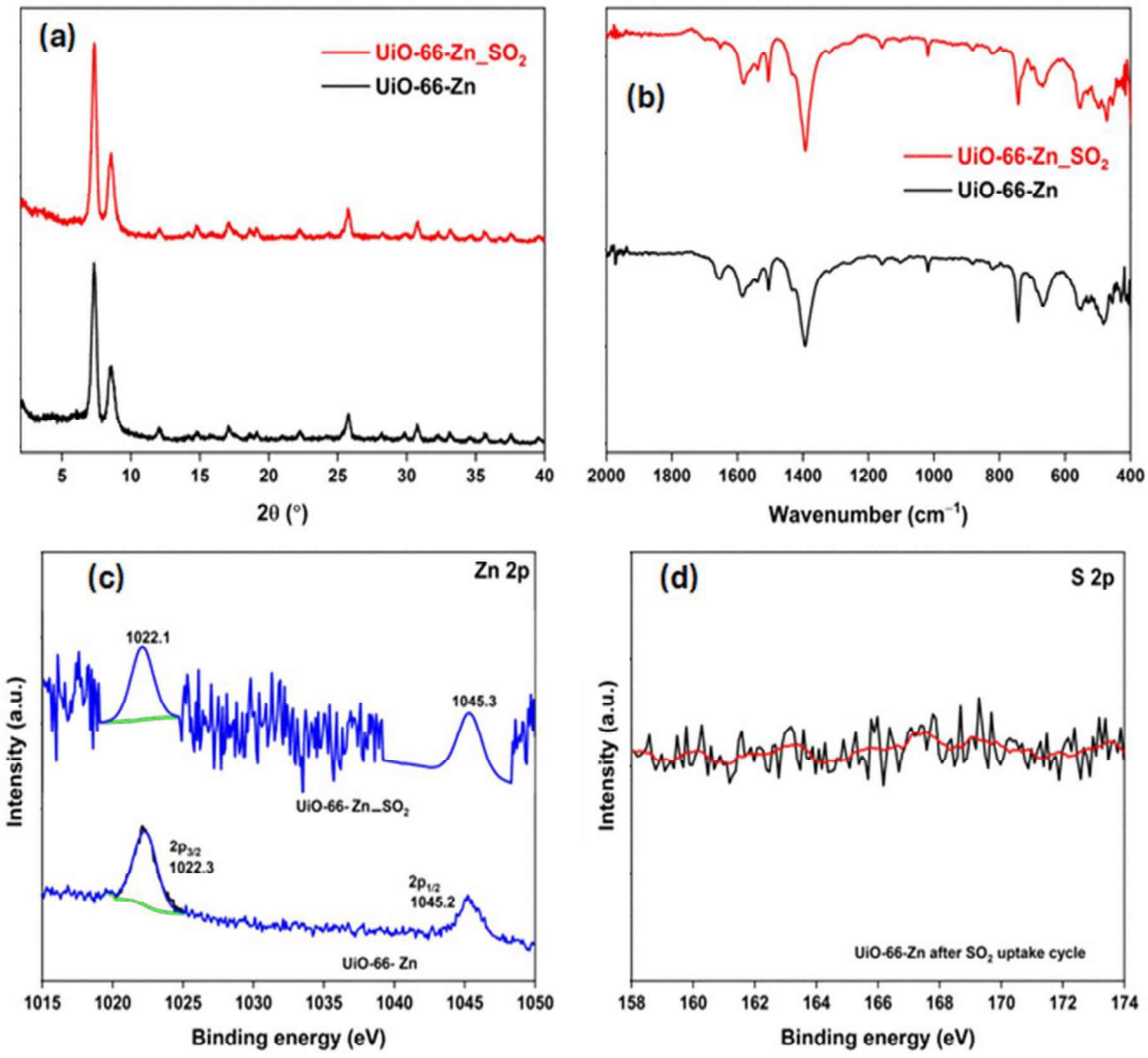

Fig. 5. (**a**) PXRD patterns; (**b**) FT-IR spectra of UiO-66-Zn before and after SO_2 exposure; high-resolution (**c**) Zn 2p; (**d**) S 2p spectra of SO_2-exposed UiO-66-Zn sample.

Conclusions

In this work, a zinc-modified zirconium-based MOF, UiO-66-Zn, was successfully synthesized via a one-step solvothermal method and comprehensively characterized using microscopic and spectroscopic techniques. Structural analyses confirmed the preservation of the UiO-66 framework after Zn incorporation, with uniform Zn distribution and stable crystallinity. UiO-66-

Zn exhibited a BET surface area of 597 m^2 g^{-1} and a maximum SO_2 uptake capacity of 4.94 mmol g^{-1} at 298 K and 1 bar, which is comparable to other highly porous Zr-MOFs. Importantly, significant adsorption was also observed in the low-pressure region (0-0.01 bar), highlighting strong host-guest interactions between SO_2 molecules and Zn sites. Post-adsorption PXRD, FT-IR, and XPS analyses demonstrated that UiO-66-Zn maintained its crystallinity and chemical integrity after SO_2 exposure, with only minor shifts in Zn 2p peaks and no permanent sulfur species detected. These results confirm the reversible nature of SO_2 adsorption and the structural robustness of the material. Overall, UiO-66-Zn combines high uptake capacity, excellent low-pressure performance, and remarkable stability, making it a promising candidate for practical desulfurization applications.

Author's Contributions

N.K.G. oversaw data curation, formal analysis, methodology, conceptualization, visualization, software, and validation. N.K.G. and K.S.K. were responsible for writing – original draft, and writing – review & editing. K.S.K. was responsible for funding acquisition, investigation, project administration, resources, and supervision.

Conflict of Interest

There are no conflicts to declare.

Acknowledgements

The authors acknowledge Prof. Ilich A. Ibarra and Dr. Eva Martínez-Ahumada at the Instituto de Investigaciones en Materiales, Universidad Nacional Autónoma de México, Ciudad de México, Mexico, for providing the DVS analyzer for recording the SO_2 adsorption-desorption isotherm. The authors are grateful for the funds provided by the “Korea Institute of Civil Engineering and Building Technology” (KICT), Republic of Korea.

References

1. A. Koutsianos, E. Kazimierska, A. R. Barron, M. Taddei and E. Andreoli, Dalton Trans., 48, 3349–3359, 2019.

2. G. W. Peterson, J. B. DeCoste, F. Fatollahi-Fard and D. K. Britt, Ind. Eng. Chem. Res., 53, 701–707, 2014.

3. A. Dhakshinamoorthy, A. Santiago-Portillo, A. M. Asiri and H. Garcia, ChemCatChem, 11, 899–923, 2019.

4. D. Cartagenova, F. A. Peixoto Esteves, N. T. Fischer, J. A. Van Bokhoven and M. Ranocchiari, Inorg. Chem. Front., 9, 70–77, 2022.

5. J. B. DeCoste, T. J. Demasky, M. J. Katz, O. K. Farha and J. T. Hupp, New J. Chem., 39, 2396–2399, 2015.

6. I. Walton, C. Chen, J. M. Rimsza, T. M. Nenoff and K. S. Walton, Cryst. Growth Des., 20, 6139–6146, 2020.

7. W. Li, J. Li, Q. Hong, Z. Liu, J. Wang, H. Xu, W. Huang, N. Yan and Z. Qu, J. Environ. Chem. Eng., 13, 116038, 2025.

8. J. Yang, Y. Zhang, M. Gao, M. Gao, K. Wang, M. Zhang, X. Wang, L. Xu, Z. Wang and B. Shen, Fuel, 370, 131853, 2024.

9. K. Tan, S. Zuluaga, H. Wang, P. Canepa, K. Soliman, J. Cure, J. Li, T. Thonhauser and Y. J. Chabal, Chem. Mater., 29, 4227–4235, 2017.

10.` Y. W. Chen, J. H. Sun, Y. Shi, Y. Ding, Q. D. Zhao, W. Xiong, C. Li, Z. F. Zhao, Y. L. Huang and L. P. Huang, Mater. Chem. Phys., 318, 129176, 2024.

11. P. Brandt, A. Nuhnen, M. Lange, J. Möllmer, O. Weingart and C. Janiak, ACS Appl. Mater. Interfaces, 11, 17350–17358, 2019.

12. S. Øien, D. Wragg, H. Reinsch, S. Svelle, S. Bordiga, C. Lamberti and K. P. Lillerud, Cryst. Growth Des., 14, 5370–5372, 2014.

13. I. Skans, M. Mnguni and P. N. Nomngongo, Anal. Sci. Adv., 2025, 6, e70023.

14. Q. Zhang, T. Yang, X. Liu, C. Yue, L. Ao, T. Deng and Y. Zhang, RSC Adv., 9, 16357–16365, 2019.

15. R. R. Solís, M. Peñas-Garzón, C. Belver, J. J. Rodriguez and J. Bedia, J. Environ. Chem. Eng., 10, 107122, 2022.

16. N. K. Gupta, J. Bae, S. Kim and K. S. Kim, Chemosphere, 274, 129789, 2021.

17. P. Brandt, S.-H. Xing, J. Liang, G. Kurt, A. Nuhnen, O. Weingart and C. Janiak, ACS Appl. Mater. Interfaces, 13, 29137–29149, 2021.

18. J. H. Carter, X. Han, F. Y. Moreau, I. Da Silva, A. Nevin, H. G. W. Godfrey, C. C. Tang, S. Yang and M. Schröder, J. Am. Chem. Soc., 140, 15564–15567, 2018.

19. T. G. Grissom, D. M. Driscoll, D. Troya, N. S. Sapienza, P. M. Usov, A. J. Morris and J. R. Morris, J. Phys. Chem. C, 123, 13731–13738, 2019.

20. P. Brandt, A. Nuhnen, S. Öztürk, G. Kurt, J. Liang and C. Janiak, Adv. Sustainable Syst., 5, 2000285, 2021.

21. J. García Ponce, M. L. Díaz-Ramírez, S. Gorla, C. Navarathna, G. Sanchez-Lecuona, B. Donnadieu, I. A. Ibarra and V. Montiel-Palma, CrystEngComm, 23, 7479–7484, 2021.

22. Y. Zhang, P. Zhang, W. Yu, J. Zhang, J. Huang, J. Wang, M. Xu, Q. Deng, Z. Zeng and S. Deng, ACS Appl. Mater. Interfaces, 11, 10680–10688, 2019.

23. Y. Zhang, Z. Chen, X. Liu, Z. Dong, P. Zhang, J. Wang, Q. Deng, Z. Zeng, S. Zhang and S. Deng, Ind. Eng. Chem. Res., 59, 874–882, 2020.

24. Y. Sun, J. Liang, P. Brandt, A. Spieß, S. Öztürk and C. Janiak, Nanoscale, 13, 15952–15962, 2021.